PNC TN9410 92-039

公開資料

DESIGN OF A CW HIGH BEAM POWER ELECTRON LINAC

February 1992

Power Reactor and Nuclear Fuel Development Corporation
Oarai Engineering Center

複製又はこの資料の入手については、下記にお問い合わせ下さい。
〒311-13　茨城県東茨城郡大洗町成田町4002
動力炉・核燃料開発事業団
大洗光学センター
技術開発部・技術管理室
Inquiries about copyright and reproduction should be addressed to : Technology Management Section, O-arai Engineering Center, Power Reactor and Nuclear Fuel Development Corporation 4002 Narita-machi, O-arai-machi, Higashi-Ibaraki, Ibaraki-Ken 311-13, Japan.

動力炉・核燃料開発事業団（Power Reactor and Nuclear Fuel Development Corporation）1992

Ⓝ

COMMERCIAL PROPRIETARY
PNC TN9410 92-039
February 1992

DESIGN OF A CW HIGH BEAM POWER ELECTRON LINAC

Y. L. Wang *

Abstract

A test CW electron linac is designed to develop a high power accelerator to treat waste radioactive material.

The linac is to be operated at the room temperature and is energized by two 1.2MW CW L-band klystrons to produce an electron beam with the energy of 10MeV and current of 100mA. The average beam power is 200KW-1MW for the duty factor 20%-100%.

In designing such high power electron linear accelerator, an accelerating section having a traveling wave resonant ring is adopted. By adopting such type of acceleration section, it became possible to choose very short length of the accelerator sections to elevate the threshold current of beam break-up (BBU) keeping the high accelerator efficiency.

In designing the linac with the traveling wave resonant ring, some special considerations and calculations are introduced.

The variational method is used to calculate the sizes and parameters of the disk-loaded accelerator structure. There is the discrepancy of the order of a few hundredth of one percent between the calculated frequency and the experimental one.

A kind of internal cooling water structure is adopted to disperse the generated heat by RF efficiently.

Currently, its components development is in progress at OEC.

* Frontier Technology Development Section
Oarai Engineering Center (OEC)
Visiting Researcher from Nanjing University, China

公　開　資　料
PNC TN9410 92-039
１９９２年　２月

連続波高ビーム出力の電子線形加速器の設計

王　元林*

要　旨

放射性物質を扱う高出力の加速器開発を目的に、試験用の連続波電子線型加速器の設計を行った。

この加速器は、室温で運転され、出力1.2MWのＬ－バンド連続波を供給する２台のクライストロンでエネルギーが投入されて、100mAの電子を10MeVに加速することが出来る。平均ビーム出力はデューテイファクター20～100％の時に200KW～1MWである。

設計では、加速管に進行波還流型の加速管を採用した。この型の加速管には、高い加速率を維持したままビームブレークアップ（ビーム散乱）の防止するため加速部を短く設計できる利点がある。これらの設計の際は、特別な工夫を加え、またそれに基づく設計計算も行った。加速管構造の寸法とパラメータの決定は変分法に基づく計算で行った。計算で得たマイクロ波の共鳴周波数は、実測値と１／100％オーダーの誤差範囲内で一致した。

現在、設計した加速器の要素開発を大洗工学センターで進めている。

* 大洗工学センター、技術開発部、フロンティア技術開発室　客員研究員
（中国、南京大学物理学部準教授）

Contents

List of Tables

List of Figures

1. Introduction

A program has been developing in order to transmute long-lived radioactive nuclides in spent fuels from nuclear reactors into short-lived or stable ones by means of reactor or accelerator. The fission products, especially, strontium-90 and cesium-137 which occupy the most part of nuclear waste from spent fuels are not suited to transmute in reactors because their neutron reaction cross-section are small. One possible way to transmute them is to use their photo nuclear reaction using an accelerator. However, a energy 100MeV continuous wave (CW) electron linac will be needed for this objective. Its beam current should be as high as possible. Now a test linac whose energy and beam current are 10MeV and 100mA, respectively, is designed, and development of its key components is in progress at OEC. The linac is energized by two 1.2MW L-band CW klystrons. In case of operation, the linac will be operated at 20% duty factor with the RF pulse length of 5ms at 50Hz, then it will be operated at a duty factor up to 100%. The beam energy spectra are less than 1%, and the width of bunch phase is less than 5 degree. In the future we will design a 100 MeV CW linac with 1A beam current .

2. Design Considerations

Features and specifications of the CW linac are as followings:

1) high duty factor (20-100%),
2) high average beam power (200kW-1MW),
3) low accelerating electrical field (1.4MV/m),
4) narrow energy spectra (<1%) and phase width (<5°), and
5) low beam emittance (π mm mrad).

For design such a high power CW linac, there are some special considerations:

1) The first important issue is to elevate the threshold current level of the beam breakup (BBU). To do this, we took the following measures:
   a) to use L-band frequency and $2\pi/3$ mode ;
   b) to use the constant gradient accelerator structure under the 100mA beam loading;
   c) to use short accelerator sections (L=1.2m) and low attenuation constant structures (τ =0.05Nepers);
   d) to use a progressive stop-band technique and

f) to use "brute force" - straightforward magnetic focusing schemes - three pairs of beam steering Helmholtz coils to inject and accelerate small cross-section beams and to maintain the trajectories as close as practicable to the central axis.

2) The second important issue is to obtain higher efficiency of the accelerator by the following measures:

a) each accelerator section is equipped with a traveling wave resonant ring.

3) The third is to get narrow energy spectra and narrow phase width and low emittance by:

a) using a RF gun,

b) using two prebunchers, and

c) using low gradient variable phase velocity traveling wave buncher.

4) The fourth is to avoid thermal deformation due to RF loss by means of:

a) enhancing the accelerator efficiency and

b) using the internal cooling water structure.

Figure 1 illustrates a schematic layout of the CW electron linac. Two klystrons energize a system of a RF gun, two prebunchers, a buncher and 7 accelerator sections. The length of each accelerator section and the buncher are 1.2m and 1.12m, respectively. Total length of this accelerator is about 16m.

3. Injector

A injector consists of a 200kV electron RF gun, two prebunchers, a buncher and an accelerator section. The beam current from the RF gun is 200mA in a quarter RF periodic (90°). The prebunchers and buncher are designed so as to avoid phase orbit cross-overs as much as possible. In the buncher the wave phase velocity varies linearly and slowly, at the first half part from 0.695C to 0.93C and in the second part from 0.93C to 1.0C.

In the injector, each part has a phase shifter and a attenuater to change its phase and input RF power to adjust the bunch phase width and energy spectra. After two prebunchers the bunch width becomes about 10 degree. The emergent bunch width from the injector is 3.8 degree.

4. Accelerator Structure

The accelerating part consists of 7 sections: one in the injector and six after the injector. Each of the accelerator section whose length is 1.2m contains thirteen $2\pi/3$ mode cavities and two coupling cavities. They are designed to have a constant gradient structure under 100 mA beam loading condition. It can make larger difference of the TM11-like mode frequency between two neighboring cavities. According to the progressive stop-band technique [1], the iris diameters in the initial region of the accelerator section are smaller than those in any preceding ones but larger than those in subsequently located ones. Table 1 lists the parameters of the disk loaded structure. Fig.2 shows the wave phase velocity, accelerating field and iris diameters of the buncher and two types of accelerator structures. The Brillouin diagrams of the accelerator structure are shown in Fig. 3. The TM11-like mode frequency and transverse shunt impedance of the cavities are calculated by the MAFIA code. Table 2 lists the TM11-like mode frequency and π mode transverse shunt impedance.

The accelerator internal cooling structure is shown in Fig.4. The cooling water passes through 8 flow paths provided in the wall of accelerator and the disks. According to the three- dimensional finite-element heat transfer and thermal stress analysis, enough cooling capacity can be obtained with 350 l/m cooling water for one accelerator section under 20% duty factor.

Using the short accelerator sections and low attenuation constant structures described, one can not only enhance the threshold current of BBU, but also can release the tolerances of the frequency, temperature and fabrication. But in this case, it will result in low electric field throughout. Therefore, we will use the traveling wave resonant rings to improve its efficiency. [2, 3, 4, 5]

5. Characteristics of Traveling Wave Resonant Ring with Linac

As presented, every accelerator section is equipped with a traveling wave resonant ring. When one calculates the parameters of the resonant ring, one must consider the accelerator response.

The simplest resonant ring is shown in Fig.5, where the multiplication factor M is defined as follows [6]:

$$M = \frac{b_4}{a_1} = \frac{jC}{1 - T\sqrt{1-C^2}\,\exp(j\beta L)} \qquad (1)$$

where C is the coupling coefficient of the directional coupler, T=exp(- αL) is voltage transmission coefficient of the ring, L is the length of the ring, α is the attenuation in nepers per meter, β is the phase constant of the ring transmission line, $\varphi=\beta L$ is the phase of the resonant ring.

The module and argument of the multiplication faction are given by Eqs. (2) and (3).

$$|M| = \frac{C}{(1+T^2(1-C^2)-2T\sqrt{1-C^2}\,COS(\varphi))^{1/2}} \tag{2}$$

$$\theta = \arg(M) = \frac{\pi}{2} - \arctan\left(\frac{T\sqrt{1-C^2}\,COS(\varphi)}{1-T\sqrt{1-C^2}\,COS(\varphi)}\right) \tag{3}$$

The graphs of module of M, $|M|$ vs. φ, and argument of M, θ vs. φ are shown in Fig. 6. One can see from Fig. 6 that if the phase (or frequency) deviates from the resonant point, the module $|M|$ and argument θ of the M change very quickly.

Let us suppose that the directional coupler has a coupling coefficient C exp(-j ψ_1) and a transmission coefficient $\sqrt{1-C^2}$ exp(-jψ_2), where $\psi_1 - \psi_2 = \pm\pi/2$, and in the ring there is some reflection having a reflection coefficient Γexp(-jθ_1) and a transmission coefficient$\sqrt{1-\Gamma^2}$ exp(-jθ_2), where $\theta_1 - \theta_2 = \pm\pi/2$, shown on Fig. 5, the field multiplication factor M will be reduced. Therefore, equation (1) becomes:

$$M = \frac{Ce^{-j\psi_1} - CT\sqrt{1-C^2}\sqrt{1-\Gamma^2}\,e^{-j(\psi_1+\varphi+\psi_2+\theta_2)}}{1-2T\sqrt{1-C^2}\sqrt{1-\Gamma^2}\,e^{-j(\varphi+\psi_2+\theta_2)} + T^2(1-C^2)\,e^{-j(2\varphi+2\psi_2)}} \tag{4}$$

From input port view the reflection is given by:

$$\Gamma_1 = \frac{b_1}{a_1} = \frac{-C^2\,T_1^2\,\Gamma\,e^{-j(2\psi_1+2\varphi_1+\theta_1)}}{1-2T\sqrt{1-C^2}\sqrt{1-\Gamma^2}\,e^{-j(\varphi+\psi_2+\theta_2)} + T^2(1-C^2)\,e^{-j(2\varphi+2\psi_2)}} \tag{5}$$

A graph of M vs. C is shown in Fig.7, and a graph of Γ_1 vs. C is shown in Fig.8. From these figures one can see that, when there is small reflection in the ring, the multiplication factor M reduces very quickly and in the input port reflection increases M^2 times. So one must match the ring carefully.

For the resonant ring with the linac shown in Fig.9, the multiplication factor with beam loading Mb is given by:

$$Mb = \frac{\sqrt{\frac{I^2R^2}{E^2}(1-e^{-\tau a_2})\,e^{-\tau}+(1-e^{-2\tau})}-\frac{IR}{E}(1-e^{-\tau a})\,e^{-\tau}\,e^{-\tau w/2}}{1-\exp(-2\tau)} \qquad (6)$$

$\tau_a = \alpha_a L_a$ is the attenuation constant of the accelerator structure, $\tau_w = \alpha_w L_w$ is attenuation constants of the waveguide, $\tau = \tau_a + \tau_w$, La the length of the accelerator, Lw is the length of the waveguide in the resonant ring, $E=\sqrt{2PR\alpha_a}$ is the electric field, I is the beam current, R is the shunt impedance.

For the optimal coupling, the coupling coefficient is C=1/Mb. There is no power transmitted to the dummy load. The accelerator has optimum efficiency.

The energy gain of the linac with the traveling wave resonant ring is given by:

$$V = MbELa\,\frac{1-\exp(-\tau a)}{\tau a} - IRLa\left(1-\frac{1-\exp(-\tau a)}{\tau a}\right) \qquad (7)$$

For our linac one section, P=250kW, I=100mA, R= 35MΩ/m, τ_a =0.05nepers and La=1.2m, we can get Mb=1.898, C=0.5265 and V=1.65 MeV.

Fig.10 and Fig.11 show the module and argument of M vs. ϕ, with different reflections Γ. The part (a) is the CW linac without the beam loading, and the part (b) with beam loading. One can see that when the reflection is a considerable value, the module of M will appear two maximums, and the argument of M will change its deviating direction. In the part (a) their change is more serious because of the lower attenuation in the resonant ring.

So during the course to tune the resonant ring, if one finds two resonant points (maximums) in a small frequency deviation, this means that there is some reflection in the resonant ring. Then one must match and tune it again.

According to the Q definition one can calculate the frequency deviation of M at the half power point.

At first from the formula (1) one can get phase deviation of M at the half power point,

$$\Delta\varphi = \arccos\left(\frac{4T\sqrt{1-C^2} - T^2(1-C^2) - 1}{2T\sqrt{1-C^2}}\right) \tag{8}$$

The dependence of phase on the frequency in the resonant ring with a linac include two parts:

for the waveguide part

$$\frac{d\varphi_w}{\varphi_w} = \frac{\lambda_g^2}{\lambda_0^2}\frac{df}{f} \tag{9}$$

for the accelerator part

$$\frac{d\varphi_a}{\varphi_a} = \frac{C}{Vga}\frac{df}{f} \tag{10}$$

total. $$d\varphi = \left(2\pi Nw\frac{\lambda_g^2}{\lambda_0^2} + 2\pi Na\frac{C}{Vga}\right)\frac{df}{f} \tag{11}$$

According to $\Delta\varphi = d\varphi$, one can get

$$Q_L = \frac{f}{2df} = \frac{2\pi Nw\frac{\lambda_g^2}{\lambda_0^2} + 2\pi Na\frac{C}{Vga}}{2\arccos\left(\frac{4T\sqrt{1-C^2} - T^2(1-C^2) - 1}{2T\sqrt{1-C^2}}\right)} \tag{12}$$

where $Nw=Lw/\lambda_g$, $Na=La/\lambda_0$, λ_g is the waveguide wavelength, λ_0 is the free space wave length, C on the numerator is the velocity of the light, Vga and Vgw are the group velocity in the accelerator and that in the waveguide respectively.

In the resonant ring with the linac the time for the wave to travel one loop is given by:

$$tf = Lw/Vgw + La/Vga \quad (13)$$

The fields in the accelerator structure build up according to the expression:

$$E = Es(1-\exp(-\omega t/2Q_L)) \quad (14)$$

where Es is the steady state value of the electric field. To the field build-up to 99.9% of Es needs time expressed as:

$$Tf = 7\ Q_L/\ (\pi f) \quad (15)$$

and the number of the step (the wave traveling one loop is one step) is given by:

$$Nf = Tf/tf \quad (16)$$

Fig.12 shows the field build-up transients for the linac with beam loading and without beam loading respectively.

For our case some results are listed in the Table 3.

6, Characteristics of Linac with Traveling Wave Resonant Ring

In analyzing the accelerator characteristics, one must consider the action of the resonant ring. Especially, for the frequency characteristic, when the frequency changing the dependence of phase on frequency is more complicated.

According to Eq.(3) and Fig.6 near the resonant point the phase of the electric field at the port 4 is strongly dependent upon the total phase of the ring.

When the frequency changes, the phase velocity of the wave in the accelerator will be changed according to Eq.(17).

$$\frac{d\beta p}{\beta p} = \left(1 - \frac{Vp}{Vg}\right) \frac{df}{f} \quad (17)$$

The change of the frequency causes the change of electron energy and energy spectrum through four ways.

The first way is that in the accelerator structure the phase of the electron

bunch which is relative to the wave will be changed step by step change of phase velocity;

The second way is that the change of the phase in the resonant ring causes the resonant ring detune according to Eq. (11), therefore, the multiplication factor M will be reduced according to Eq. (2). Then the electric field in the accelerator structure will go down;

The third way is that the change of the phase in the resonant ring causes change of the phase between the wave and the electron buncher at input point according to Eqs. (11) and (3);

The last way is that when the frequency changes the phase which the wave transmits along waveguide from the klystron to the accelerator structure will be changed.

For the general electron linac, the frequency change causes the change of the electron energy and energy spectrum only by the first way and the last way. For our linac with traveling wave resonant rings, we must consider all four factors. According to our calculation the third and second factors are more considerable.

Fortunately, if one uses the phase control system to keep the resonant ring at resonance, the second and third factors can be offset. In the case of using the phase lock loop, the last factor will be set-off. The first factor can not be offset by some way, but for our case using the short accelerator sections and the low attenuation constant structures the dependence of the electron energy and energy spectrum on the frequency is not so strong.

Using different input parameters of deviation we calculate the longitudinal dynamics to get the characteristics of the accelerator. Fig. 13, Fig. 14, Fig. 15 and Fig. 16 show the frequency characteristic, injection characteristic, power characteristic and beam loading characteristic of the linac with the resonant rings, respectively.

During above calculations one must consider that when some input parameter changes the field multiplication factor Mb changes.

From these characteristics one can see that, if the energy stability is limited in 1%, and the phase width of the beam buncher is in 5° , the tolerance of the klystron power is in 250±3kW, the tolerance of the voltage of the klystron power supply is 90±0.9kV, the tolerance of injection voltage in 200±4kV, the tolerance of beam current is 100±1.5mA and the tolerance of the frequency is 1249.135± 0.02MHz. The phase control accuracy is ±2° .

7. RF System

The first klystron energizes the buncher and three accelerator sections with three 3dB couplers and fed RF power to the RF gun and prebunchers with 10dB coupler from the buncher branch. The second klystron energizes four accelerator sections with three 3dB couplers. Using 3dB directional coupler can cancel some reflection which come from two resonant rings.

The RF power fed to the each accelerator section is 250kW, to the buncher 220kW.

In the each resonant ring there are one phase shifter to keep the ring at resonance and one stub tuner to match the ring. There are two phase lock loops to keep the phase relationship between the wave and electrons bunch for each klystron. Between the first klystron and the buncher and the first accelerator section there are phase shifters. Between the klystrons and other accelerator sections there is no phase shifter. The lengths of waveguide are carefully controlled to give the correct phase relation between each section at the design frequency and temperature.

8. Beam Transport System

In order to get high quality and high intensity beam we use a RF gun. The diameter of the cathode is 5mm.

After the RF gun there is a vacuum valve. We insert two thin lenses between the valve and prebunchers, on the buncher and first accelerator section we use solenoid coils and between the accelerator sections we use Q magnets. There are three beam monitors and steering coils in front of the buncher, the first and the fourth accelerator sections.

Fig. 17 shows the calculation results of the longitudinal dynamics and transverse motions of electrons.

9. Design Results

Principal design parameters of this linac are listed in Table 4.

10. Some Results of Experiments

Using the variational method [7] we calculated the sizes and parameters of the disk-loaded accelerator structure shown in Fig.18. So far, we have manufactured some test cavities and a test accelerator section. We also measured the frequency, group velocity and Q value. Good agreement has been found between calculation and experimental values. The discrepancy was the order of a few hundredth of one percent between computations of the guide diameters or frequency and the experiments. The Table 5 and Table 6 show them.

Now we are manufacturing an accelerator section and a resonant ring. After that we will do high power test. The important things are to check the field multiplication factor M in the resonant ring with the accelerator section and the heat dissipation in the accelerator structure.

11. Acknowledgements

Author wishes to thank Prof. I.Sato, who gives author very good directions and helpful discussions and to thank all of our accelerator group members who give helpful discussions. Author is much indebted to our leads Dr.Sasao, Dr. Himeno and Dr.Haga who give author a good research condition and good directions.

References

1) W.Bertorzzi et al. IEEE Trans.Nucl.Sci.Vol.NS-14, No.3, 191, 1967
2) Y.L.Wang, IEEE Trans.Nucl.Sci.Vol.NS-28, No.3, 3526, 1981
3) Y.L.Wang, IEEE Trans.Nucl.Sci.Vol.NS-30, No.4, 3024, 1983
4) I.Sato, Proceedings of the 6th Symposium on Accelerator Science and Technology. 1987 Tokyo JAPAN P.95
5) Y.L.Wang and I.Sato, Proc. of the 14th Linac Accelerator Meeting in JAPAN, September 7-9, 1989, 302
6) S.J.Miller, The Microwave Journal, Sep. 1960, P.50
7) M. Nakamura, Japanese Journal of Applied Physics, Vol. 7, No.3, Narch (1968) 257

Table 1. PARAMETERS OF CW LINAC CAVITES

(L-BAND F=1249.135 Mllz)

Buncher

NO.	BETA	a (mm)	b (mm)	D (mm)	T (mm)	R (MΩ/m)	Q	ALPHA (Neper/m)	Vg/C
1	0.7064	31.20	97.2955	56.51	12.00	16.16	14565	0.03978	0.02258
2	0.7296	31.45	97.2300	58.37	12.00	17.27	14981	0.03722	0.02347
3	0.7536	31.65	97.1438	60.29	12.00	18.46	15401	0.03504	0.02425
4	0.7784	31.85	97.0579	62.27	12.00	19.70	15823	0.03303	0.02504
5	0.8040	32.00	96.9530	64.32	12.00	21.01	16247	0.03134	0.02570
6	0.8305	32.15	96.8491	66.44	12.00	22.36	16675	0.02978	0.02635
7	0.8578	32.30	96.7466	68.62	12.00	23.75	17104	0.02832	0.02701
8	0.8860	32.45	96.6453	70.88	12.00	25.18	17536	0.02699	0.02765
9	0.9151	32.55	96.5277	73.21	12.00	26.67	17969	0.02588	0.02814
10	0.9348	32.65	96.4635	74.78	12.00	27.65	18256	0.02511	0.02855
11	0.9445	32.65	96.4156	75.56	12.00	28.17	18395	0.02486	0.02861
12	0.9544	32.60	96.3511	76.35	12.00	28.27	18533	0.02474	0.02854
13	0.9643	32.55	96.2873	77.15	12.00	29.28	18672	0.02462	0.02847
14	0.9744	32.50	96.2243	77.95	12.00	29.84	18810	0.02451	0.02838
15	0.9845	32.45	96.1622	78.76	12.00	30.40	18949	0.02440	0.02830
16	0.9948	32.40	96.1007	79.58	12.00	30.97	19087	0.02430	0.02822

Accelerator Sections 1-3

NO.	BETA	a (mm)	b (mm)	D (mm)	T (mm)	R (MΩ/m)	Q	ALPHA (Neper/m)	Vg/C
1	1.0000	30.00	95.3398	80.00	12.00	32.96	19117	0.03100	0.02208
2	1.0000	29.85	95.2900	80.00	12.00	33.06	19115	0.03152	0.02172
3	1.0000	29.70	95.2530	80.00	12.00	33.17	19113	0.03205	0.02136
4	1.0000	29.55	95.2100	80.00	12.00	33.28	19110	0.03259	0.02101
5	1.0000	29.40	95.1673	80.00	12.00	33.39	19108	0.03314	0.02066
6	1.0000	29.25	95.1250	80.00	12.00	33.50	19106	0.03371	0.02032
7	1.0000	29.10	95.0829	80.00	12.00	33.61	19104	0.03428	0.01998
8	1.0000	28.95	95.0411	80.00	12.00	33.72	19102	0.03487	0.01965
9	1.0000	28.80	94.9987	80.00	12.00	33.83	19099	0.03548	0.01931
10	1.0000	28.65	94.9586	80.00	12.00	33.94	19097	0.03608	0.01899
11	1.0000	28.50	94.9177	80.00	12.00	34.05	19095	0.03673	0.01866
12	1.0000	28.35	94.8772	80.00	12.00	34.16	19093	0.03738	0.01833
13	1.0000	28.20	94.8370	80.00	12.00	34.27	19091	0.03806	0.01801
14	1.0000	28.05	94.7971	80.00	12.00	34.38	19089	0.03874	0.01769
15	1.0000	27.90	94.7575	80.00	12.00	34.49	19087	0.03945	0.01738

Accelerator Sections 4-7

NO.	BETA	a (mm)	b (mm)	D (mm)	T (mm)	R (MΩ/m)	Q	ALPHA (Neper/m)	Vg/C
1	1.0000	28.33	94.8637	80.00	12.00	34.20	19092	0.03760	0.01823
2	1.0000	28.15	94.8236	80.00	12.00	34.31	19090	0.03828	0.01791
3	1.0000	28.00	94.7838	80.00	12.00	34.42	19088	0.03896	0.01759
4	1.0000	27.85	94.7443	80.00	12.00	34.53	19086	0.03964	0.01730
5	1.0000	27.70	94.7051	80.00	12.00	34.64	19084	0.04041	0.01697
6	1.0000	27.55	94.6662	80.00	12.00	34.75	19082	0.04116	0.01666
7	1.0000	27.40	94.6276	80.00	12.00	34.86	19080	0.04193	0.01635
8	1.0000	27.20	94.5767	80.00	12.00	35.01	19078	0.04297	0.01596
9	1.0000	27.00	94.5263	80.00	12.00	35.16	19075	0.04402	0.01558
10	1.0000	26.80	94.4764	80.00	12.00	35.30	19073	0.04520	0.01518
11	1.0000	26.60	94.4271	80.00	12.00	35.45	19070	0.04635	0.01480
12	1.0000	26.40	94.3783	80.00	12.00	35.63	19069	0.04727	0.01452
13	1.0000	26.20	94.3301	80.00	12.00	35.75	19063	0.04855	0.01405
14	1.0000	26.00	94.2824	80.00	12.00	35.89	19062	0.05015	0.01396
15	1.0000	25.80	94.2353	80.00	12.00	36.04	19061	0.05148	0.01333

Table 2. Parameters of TM11-like mode

a (mm)	b (mm)	D (mm)	t (mm)	$f\pi$ (MHz)	$f_2\pi/3$ (MHz)	$f\pi/3$ (MHz)	fo (MHz)	$R_\perp(\pi)$ (MΩ/m)	$Q_.(\pi)$
30.00	95.34	80.00	12.00	1835.8	1846.1	1875.1	1899.2	22.39	31080
29.10	95.08	80.00	12.00	1846.9	1856.8	1883.8	1904.9	23.22	27440
28.20	94.84	80.00	12.00	1858.3	1867.9	1892.4	1910.2	24.13	27590
27.90	94.75	80.00	12.00	1862.2	1871.6	1895.4	1912.3	24.42	27670
28.33	94.96	80.00	12.00	1858.3	1867.9	1892.4	1910.2	23.12	27590
27.20	94.57	80.00	12.00	1868.2	1877.0	1898.6	1913.1	24.95	27760
26.40	94.38	80.00	12.00	1882.5	1892.1	1912.8	1921.6	25.46	27720
25.80	94.24	80.00	12.00	1887.5	1895.4	1913.8	1925.4	25.89	27780

Table 3. Parameters of the Resonant Ring

M	C	QL	tf(μs)	Tf(μs)	Nf	
1.8983	0.5268	3276.4	0.2738	5.8	21	with beam loading
2.6890	0.5268	4908.1	0.2738	8.7	32	without beam loading
3.0848	0.3242	9667.5	0.2738	17.2	63	without beam loading at optimal coupling

Table 4. Principal Design Parameters of the CW Linac

	Operating frequency	1249.135 MHz
	Number of Klystron	2
	RF power of a Klystron	1.2 MW
	Number of accelerator section	8
	Overall length	16 m
Injector	Gun voltage	200 kV
	Beam current	200 mA

Accelerator

	Buncher	Accelerator(1-3)	Accelerator(4-7)
Length	1.12m	1.2m	1.2m
Mode	$2\pi/3$	$2\pi/3$	$2\pi/3$
Number of cavities	16	15	15
2a	62.4-64.8	60.0-55.8	56.6-51.6mm
Shunt impedance	16.2-30.9	32.9-34.5	34.2-36.1MΩ/m
Group velocity(Vg/c)	.022-.028	.022-.017	.018-.013
Average Q	17500	19100	19100
Attenuation	0.0316	0.0455	0.0567Neper
Coupling coefficient	0.417	0.50	0.553
Multiplication	2.398	2.001	1.89

Overall performance specification

Energy	13.8 Mev
Beam current	100 mA
Energy spectra	0.38 %
Bunch width	3.6°
Beam emittance	3.2 mm mrad
Efficiency	69.5%

Table 5. L-band Cavities Sizes (f=1249.135MHz)*

Beta		2a=50.0	2a=54.0	2a=58.0	2a=62.0	2a=66.0
1.0	2b(cal.)	188.104	189.053	190.110	191.276	192.552
	2b(meas.)	188.067	189.017	190.062	191.222	192.511
0.9	2b(cal.)	188.627	189.679	190.849	192.136	193.539
	2b(meas.)	188.594	189.652	190.808	192.089	193.510
0.8	2b(cal.)	189.284	190.461	191.765	193.195	194.748
	2b(meas.)	189.254	190.436	191.729	193.152	194.728
0.7	2b(cal.)	190.126	191.455	192.920	194.519	196.248
	2b(meas.)	190.099	191.434	192.888	194.480	196.234

* All values under 20℃ and in the vacuum

Table 6. The Group Velocities of Each Cavity in the Constant Gradient Structure

No.	2a(mm)	Vg/C (cal.)	Vg/C (Meas.)	△Vg/C
1	56.30	0.01791	0.01757	0.00034
2	56.00	0.01760	0.01725	0.00035
3	55.70	0.01730	0.01693	0.00037
4	55.40	0.01697	0.01662	0.00035
5	55.10	0.01667	0.01631	0.00036
6	54.80	0.01636	0.01601	0.00035
7	54.40	0.01597	0.01561	0.00036
8	54.00	0.01559	0.01521	0.00038
9	53.60	0.01518	0.01482	0.00036
10	53.20	0.01481	0.01444	0.00037
11	52.80	0.01452	0.01406	0.00046
12	62.40	0.01405	0.01369	0.00036
13	52.00	0.01369	0.01332	0.00037
14	51.60	0.01334	0.01296	0.00038

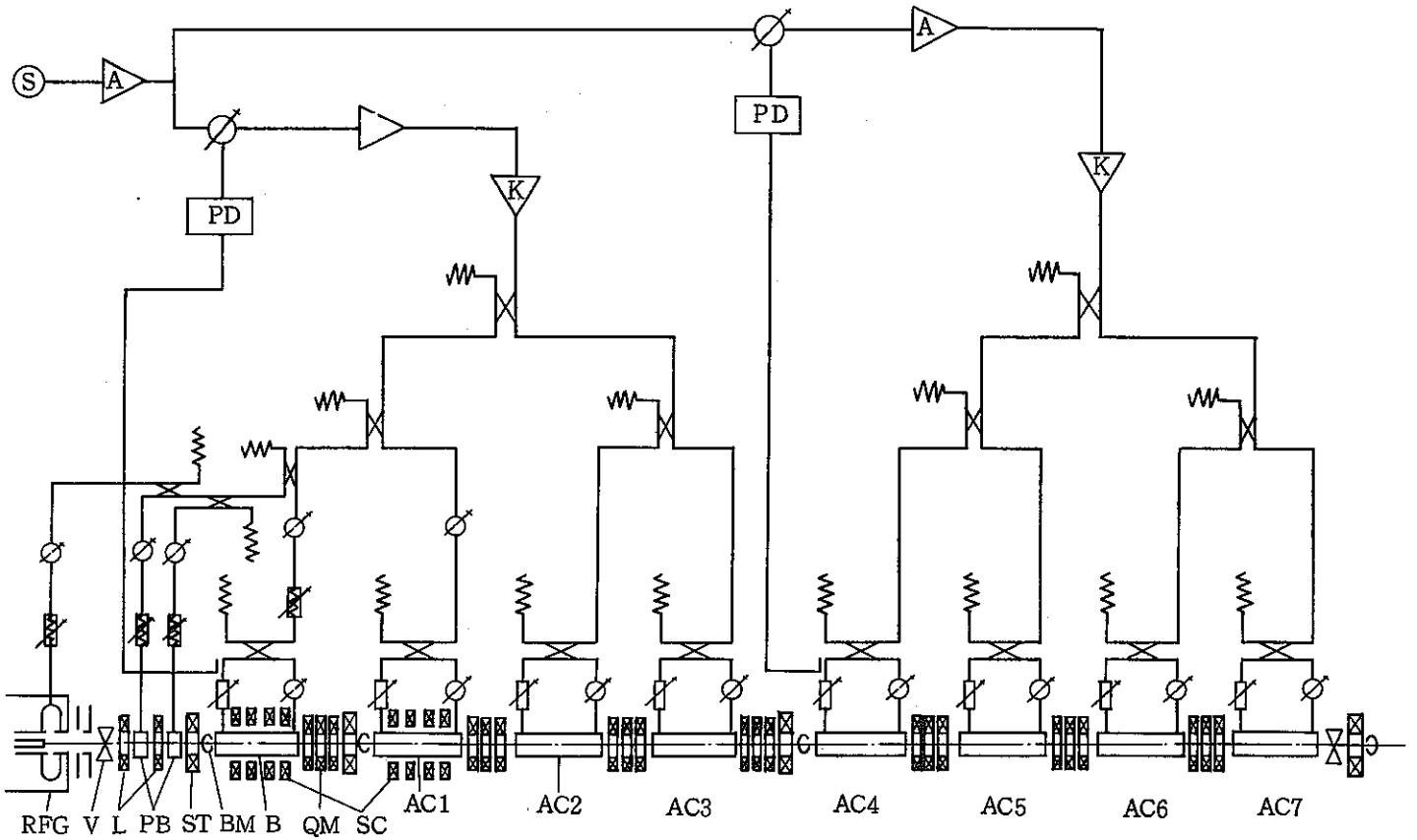

- Attenuator - Matcher - Phase Shifter

A - Amplifier K - Klystron RFG - RF Gun PB - Prebuncher B - Buncher
AC - Accelerator V - Valve L- Lens SC - Solenoils Coils ST - Steering Coils
PD - Phase Detector S - Signal Genertor QM - Q Magnet BM - Beam Monitor

Fig. 1, Schematic layout of the CW electron linac

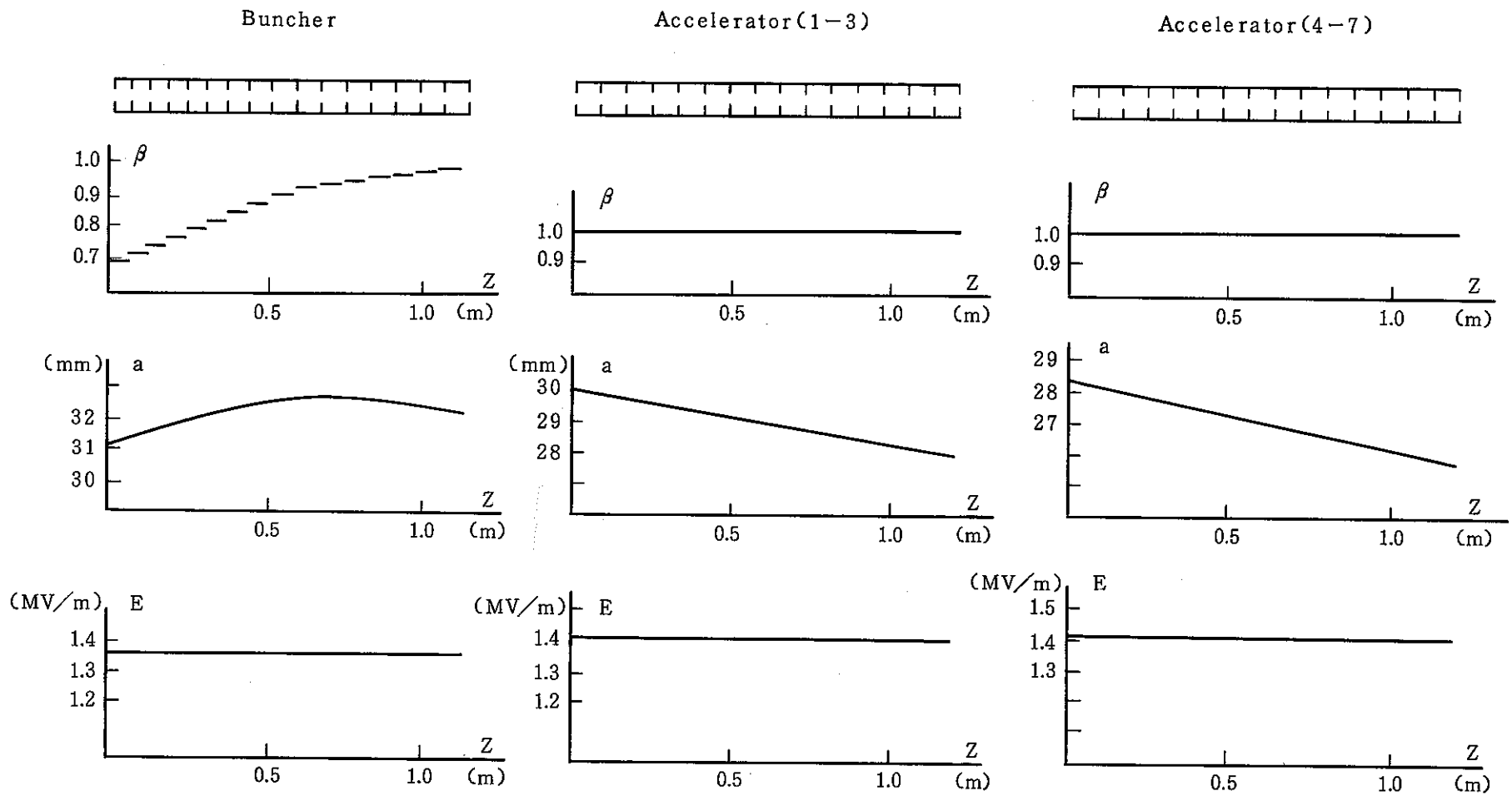

Fig. 2, Phase velocity, iris diameter and accelerating field in the accelerator sections

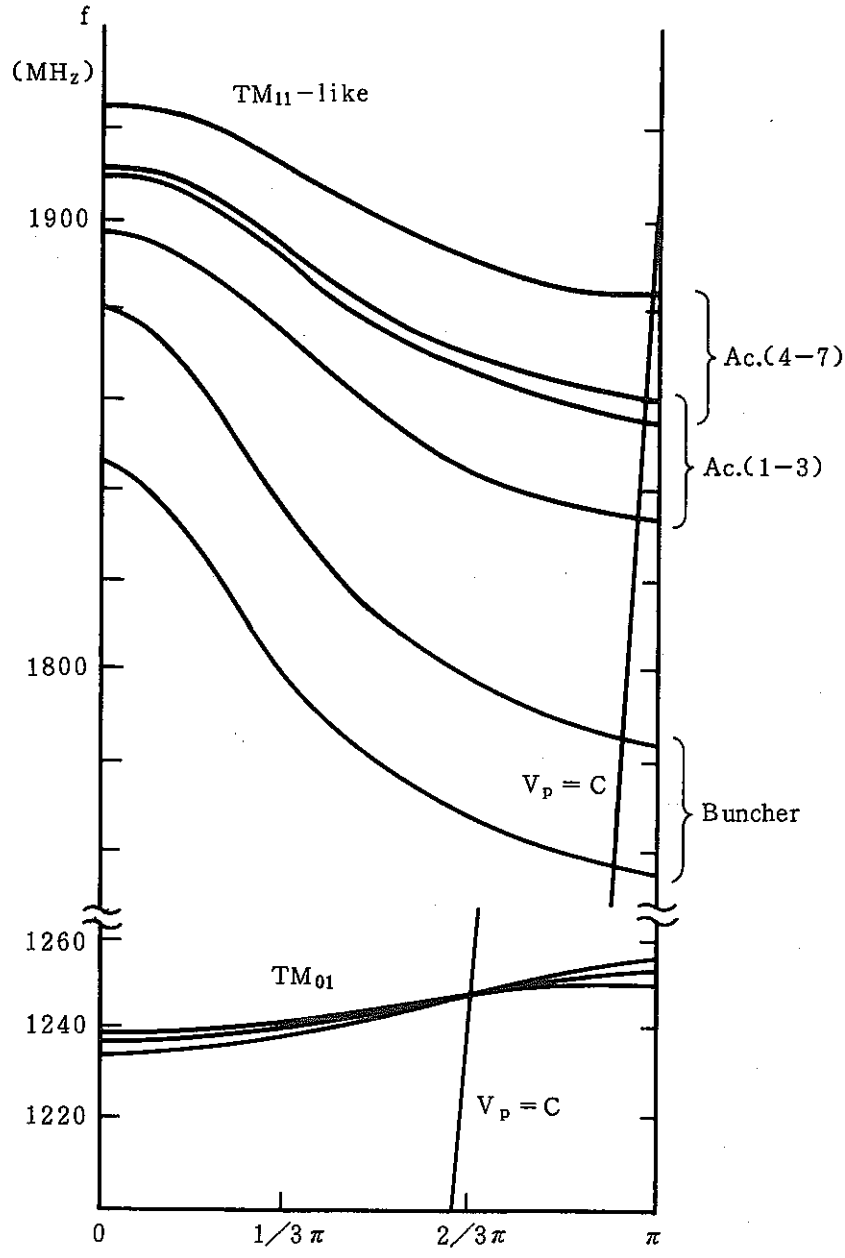

Fig. 3, The Brillouin diagram of the accelerator structure

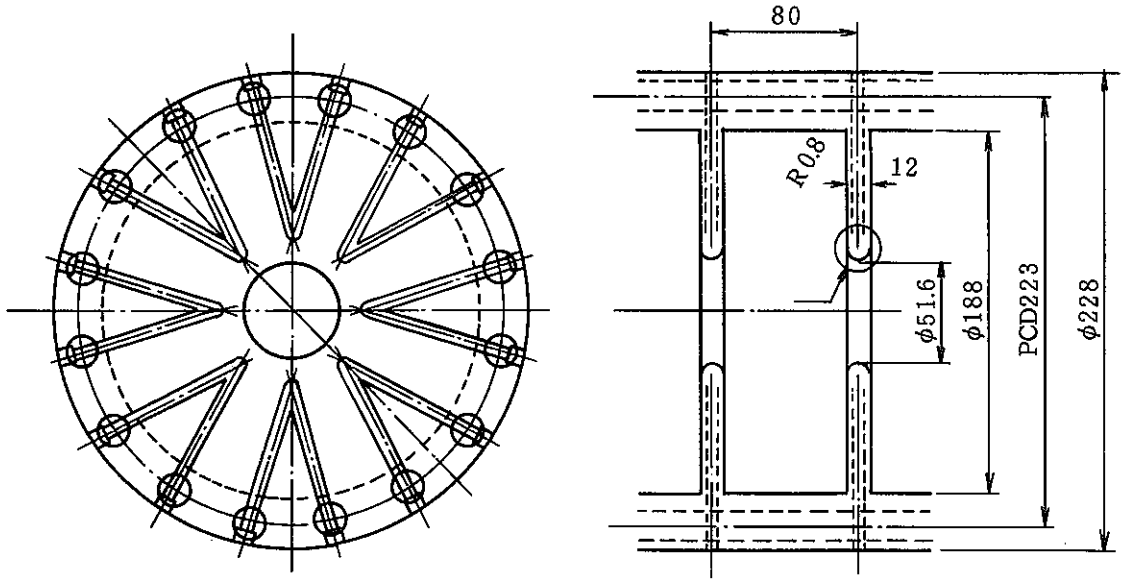

Fig. 4, The accelerator internal cooling structure

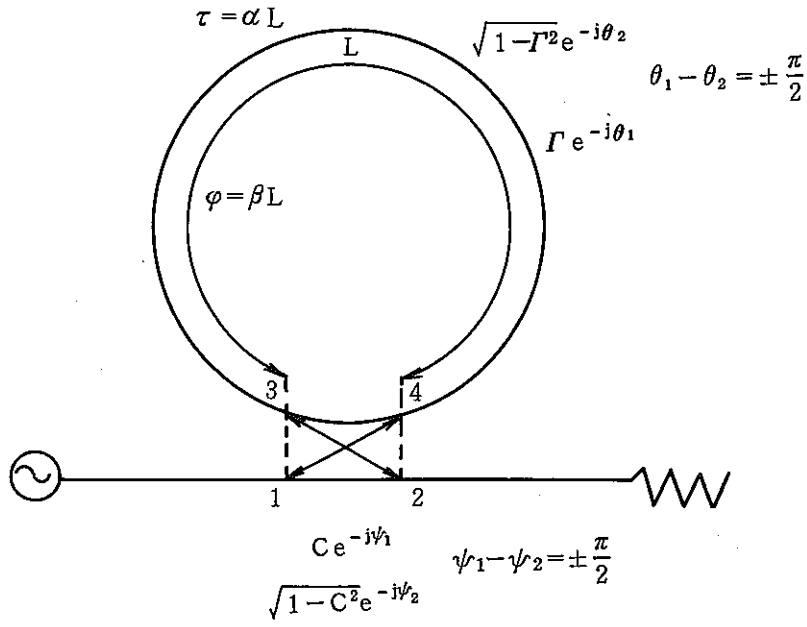

Fig. 5, The simplest resonant ring

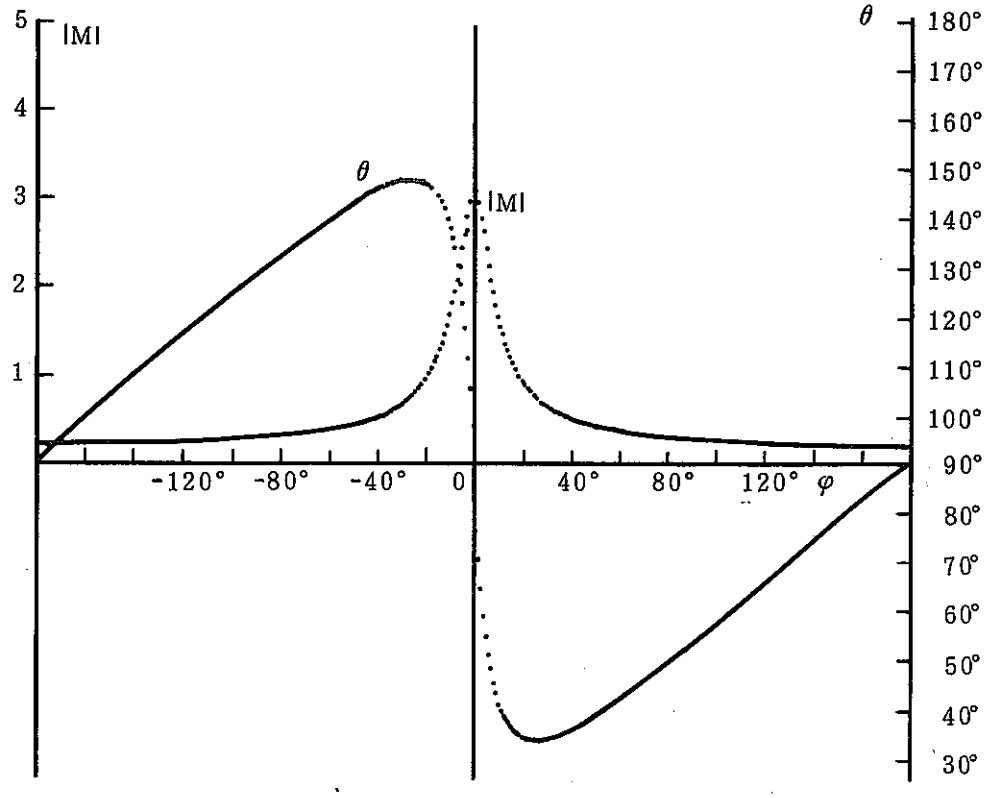

Fig. 6, The module and argument of the multiplication factor M vs. the phase of the resonant ring φ

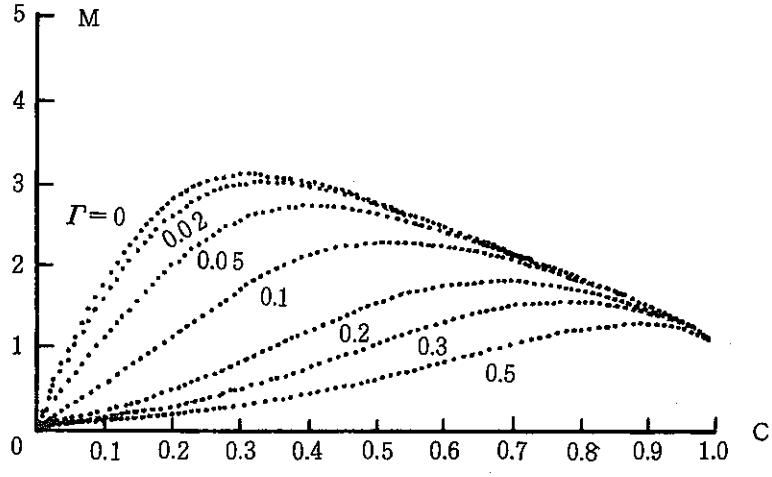

Fig. 7, The graph of M vs. C with different reflection Γ in the resonant ring

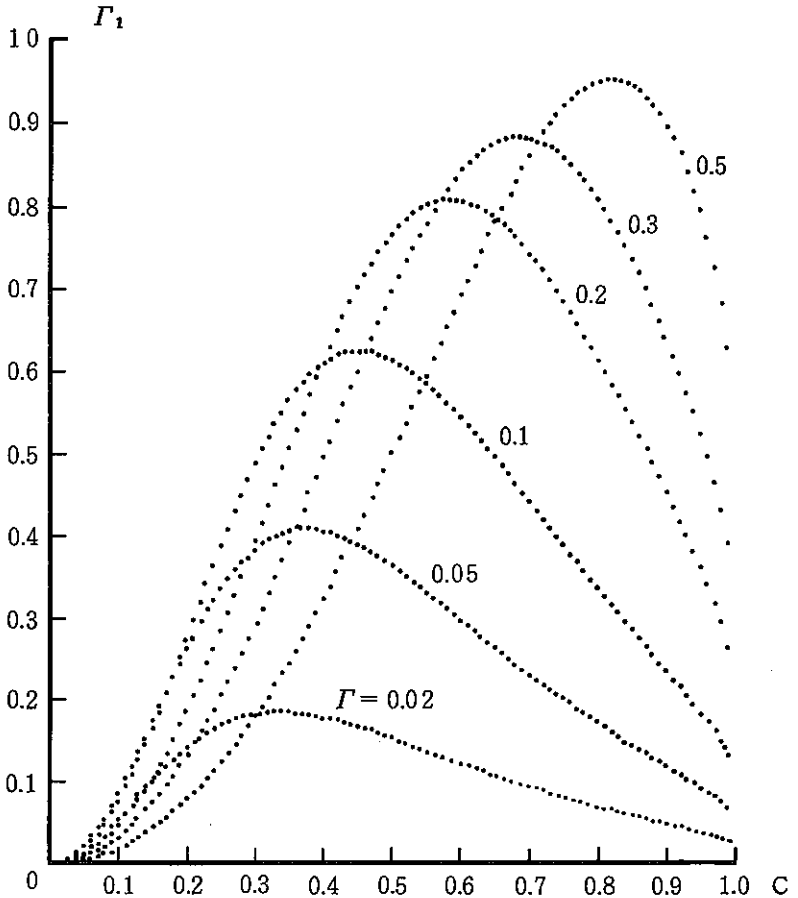

Fig. 8. The graph of Γ_1 vs. C with different reflections Γ in the resonant ring

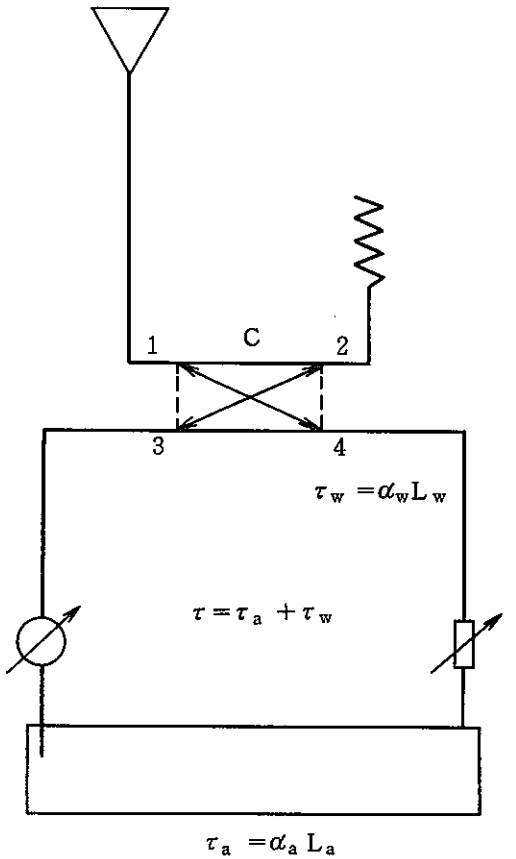

Fig. 9. The resonant ring with the linac

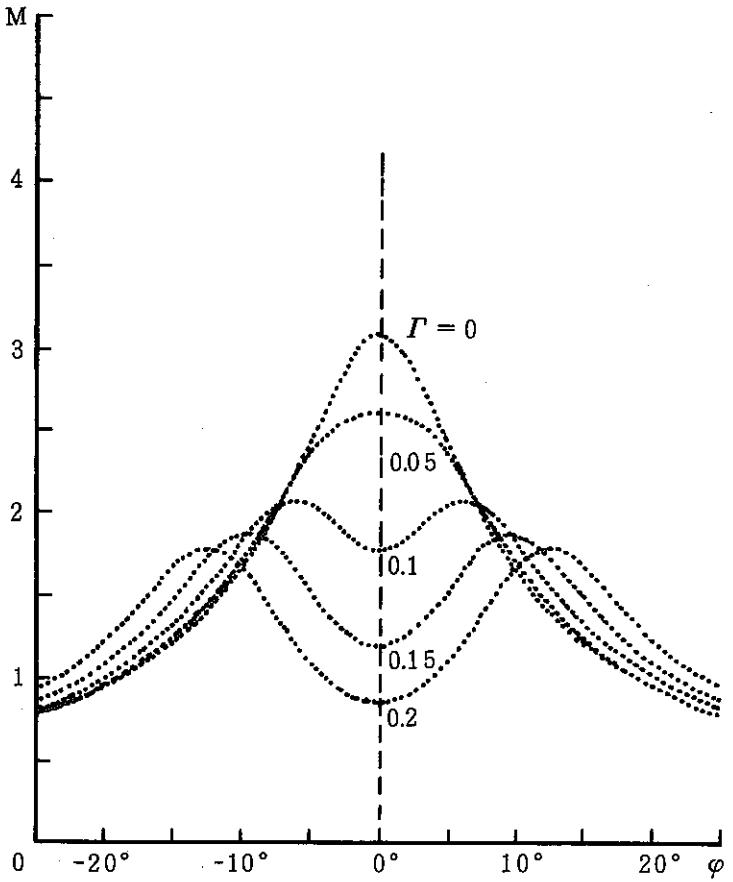

a), the resonant ring with the linac
without beam loading

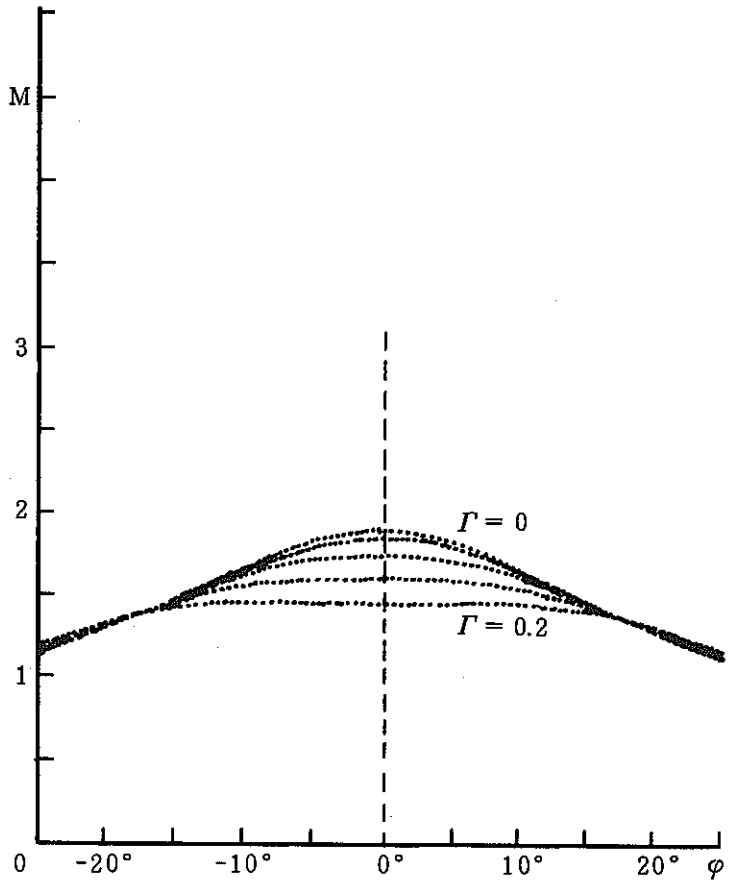

b), the resonant ring with the linac
with beam loading

Fig. 10. The multiplication factor M vs φ
with different reflection Γ in the resonant ring

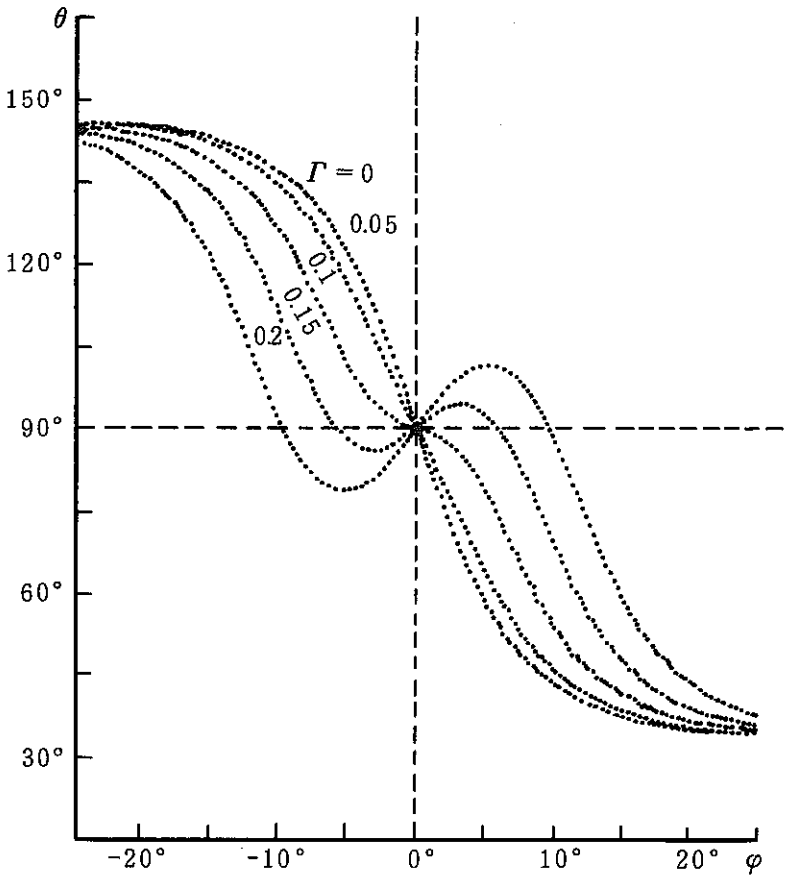

a), the resonant ring with the linac
without beam loading

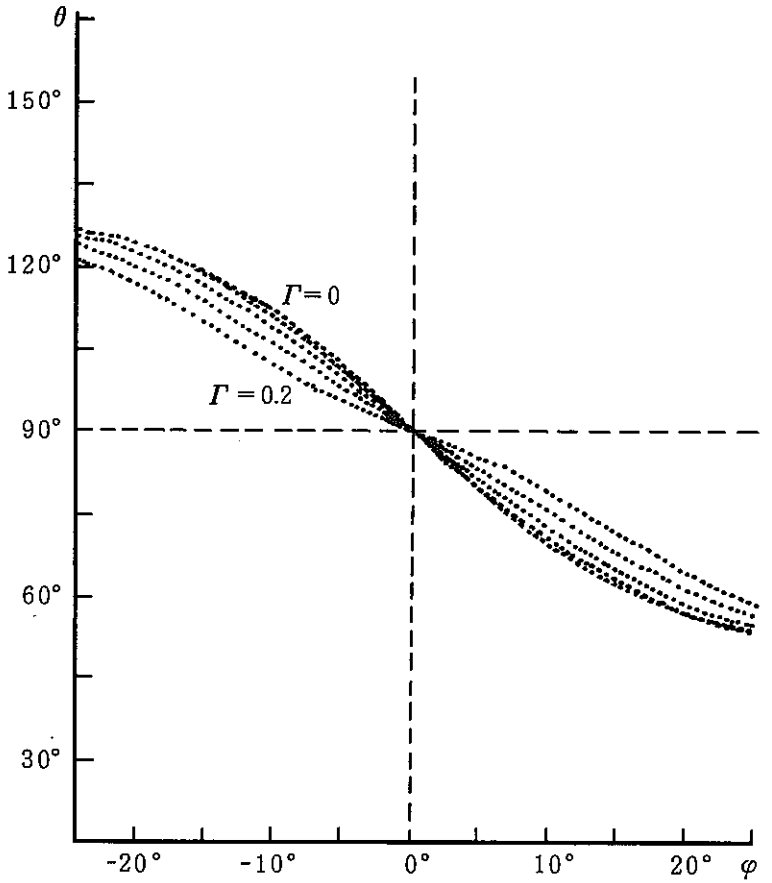

b), the resonant ring with the linac
with beam loading

Fig. 11. The argument of M vs. φ
with different reflection Γ in the resonant ring

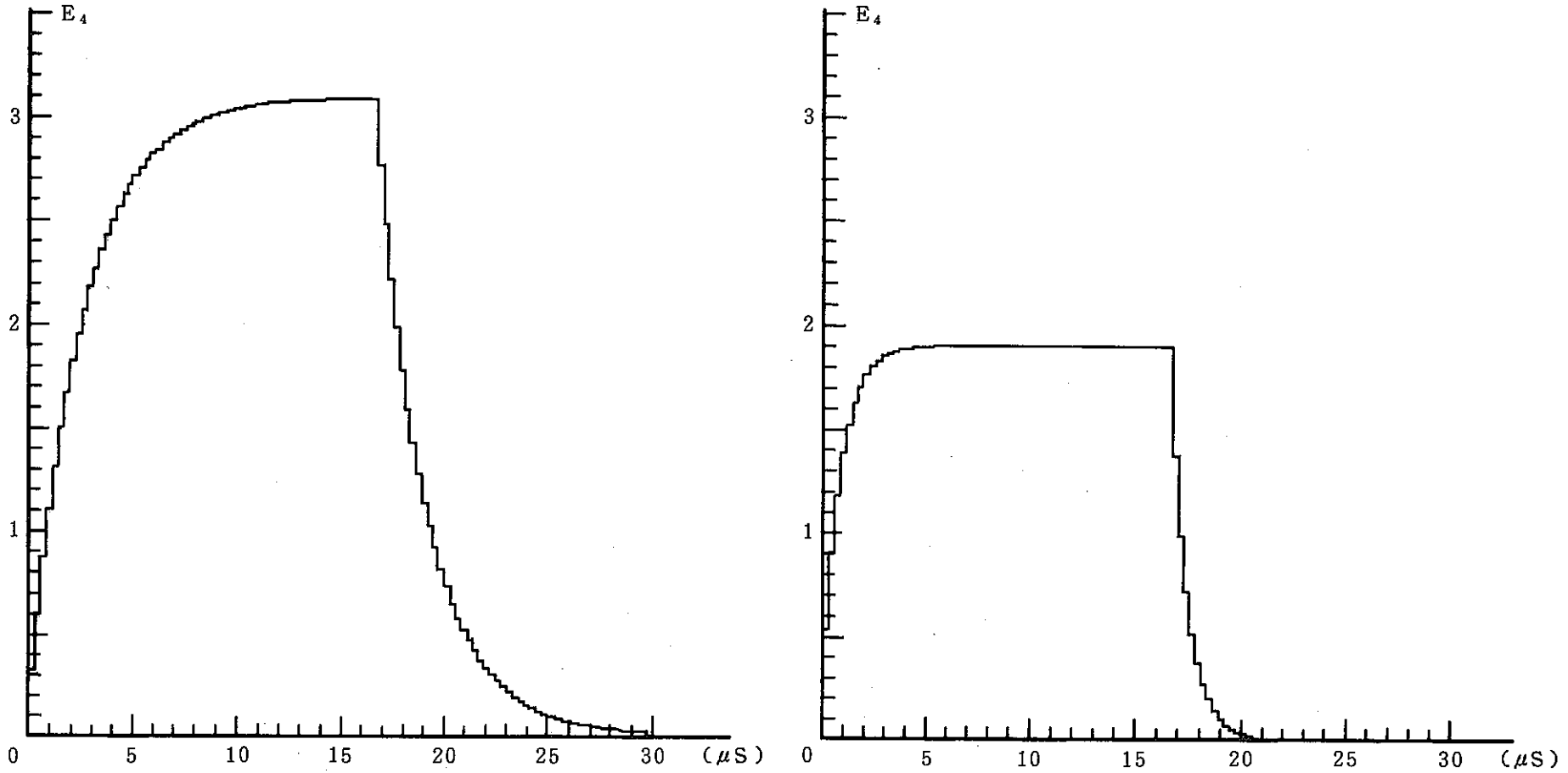

a), the resonant ring with the linac without beam loading

b), the resonant ring with the linac with beam loading

Fig. 12. The field build-up in the resonant ring
(one step corresponds to the wave traveling one loop)

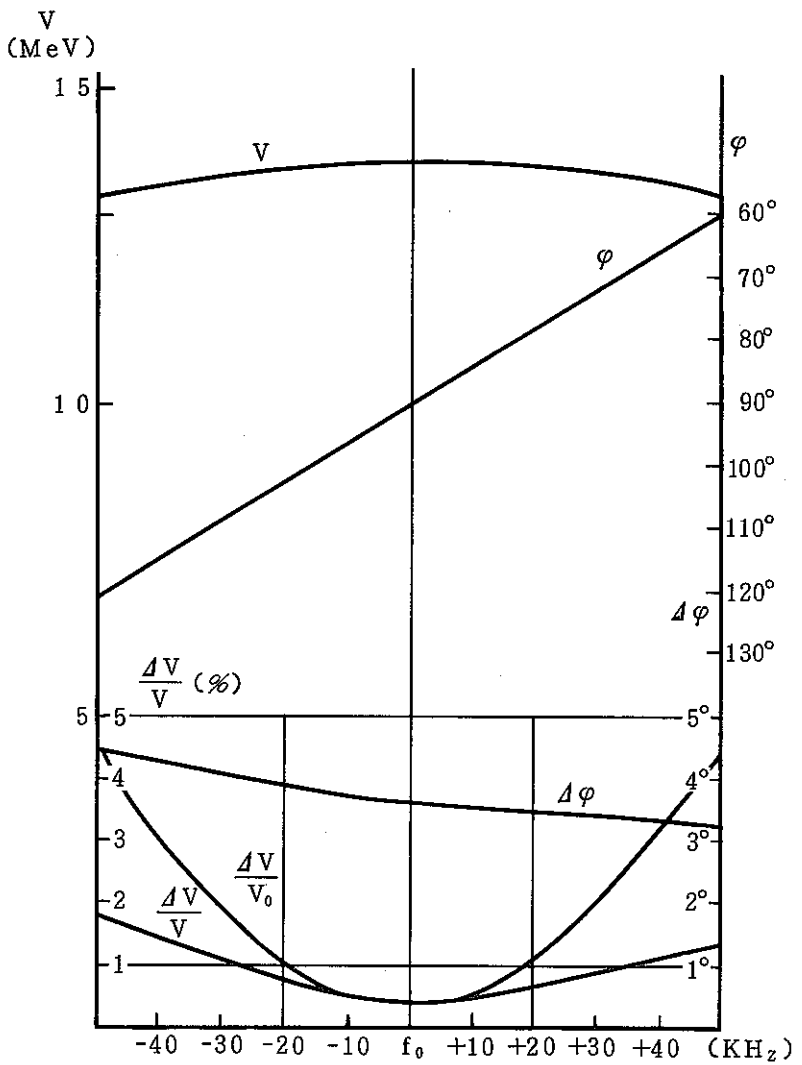

Fig. 13. Frequency characteristic of the linac with resonant ring

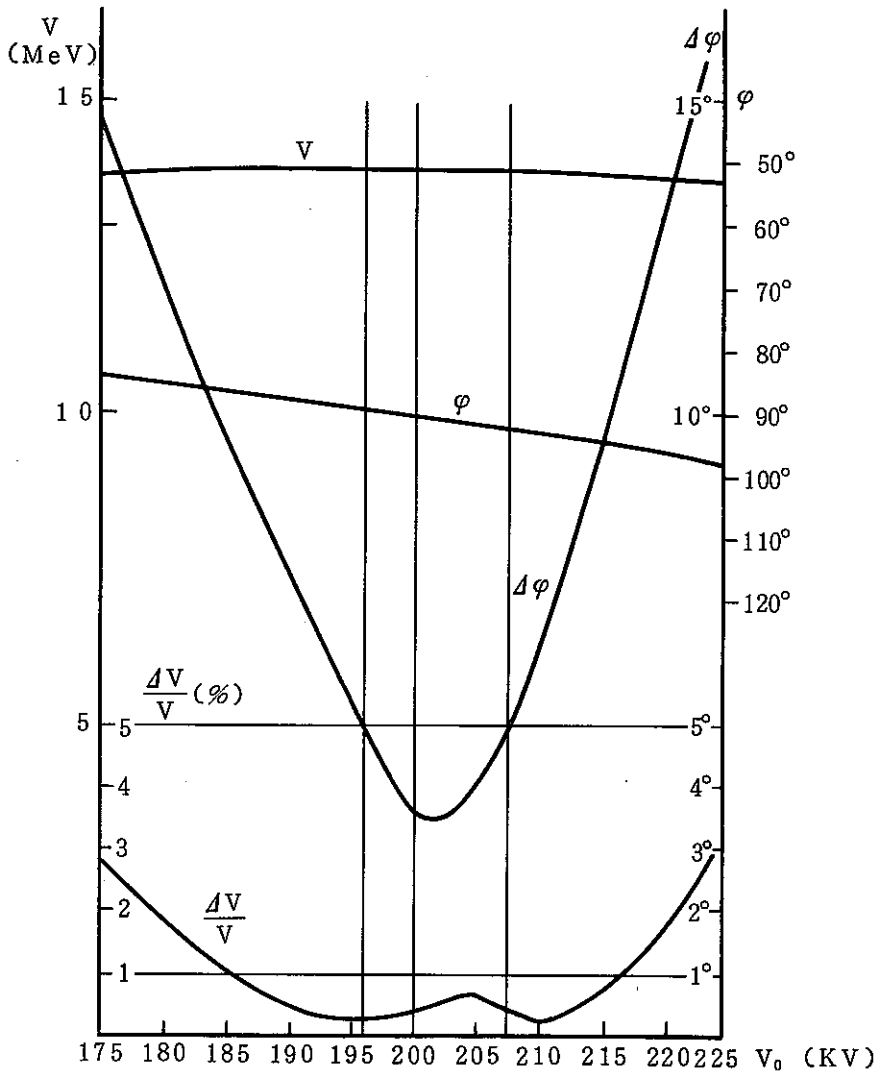

Fig. 14. Injection characteristic of the linac with resonant ring

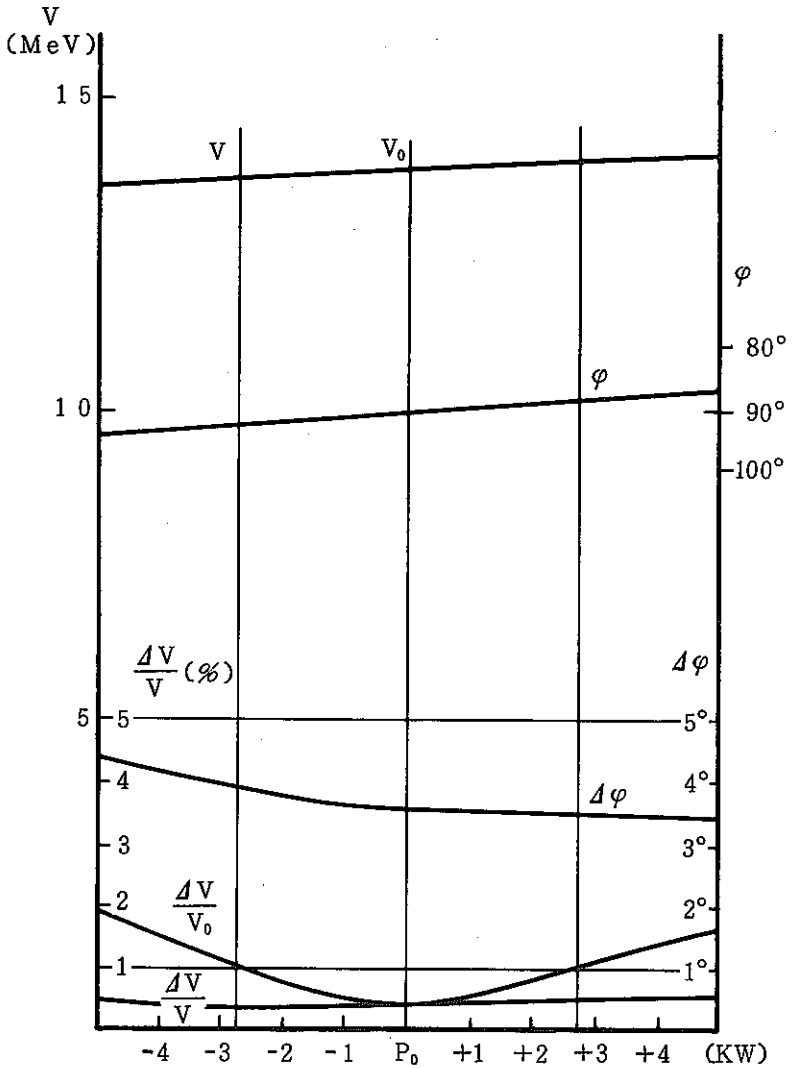

Fig. 15. Power characteristic
of the linac with resonant ring

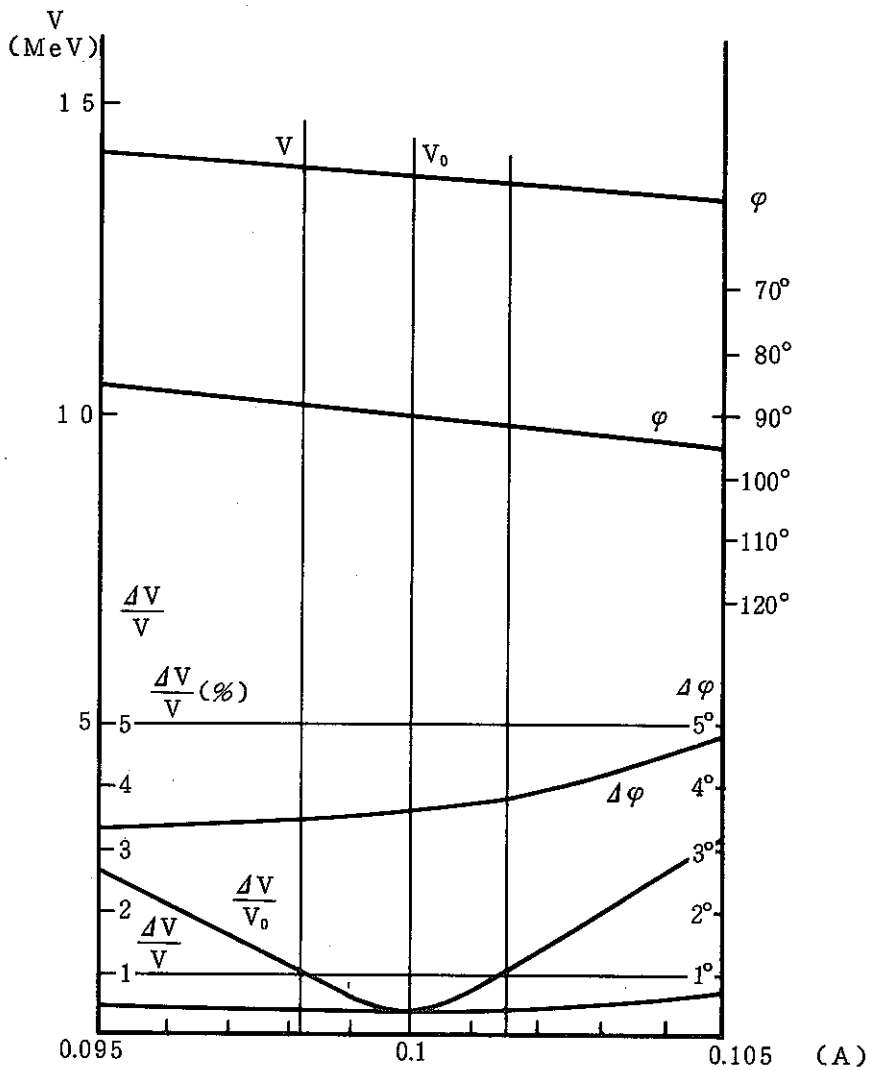

Fig. 16. Beam loading characteristic
of the linac with resonant ring

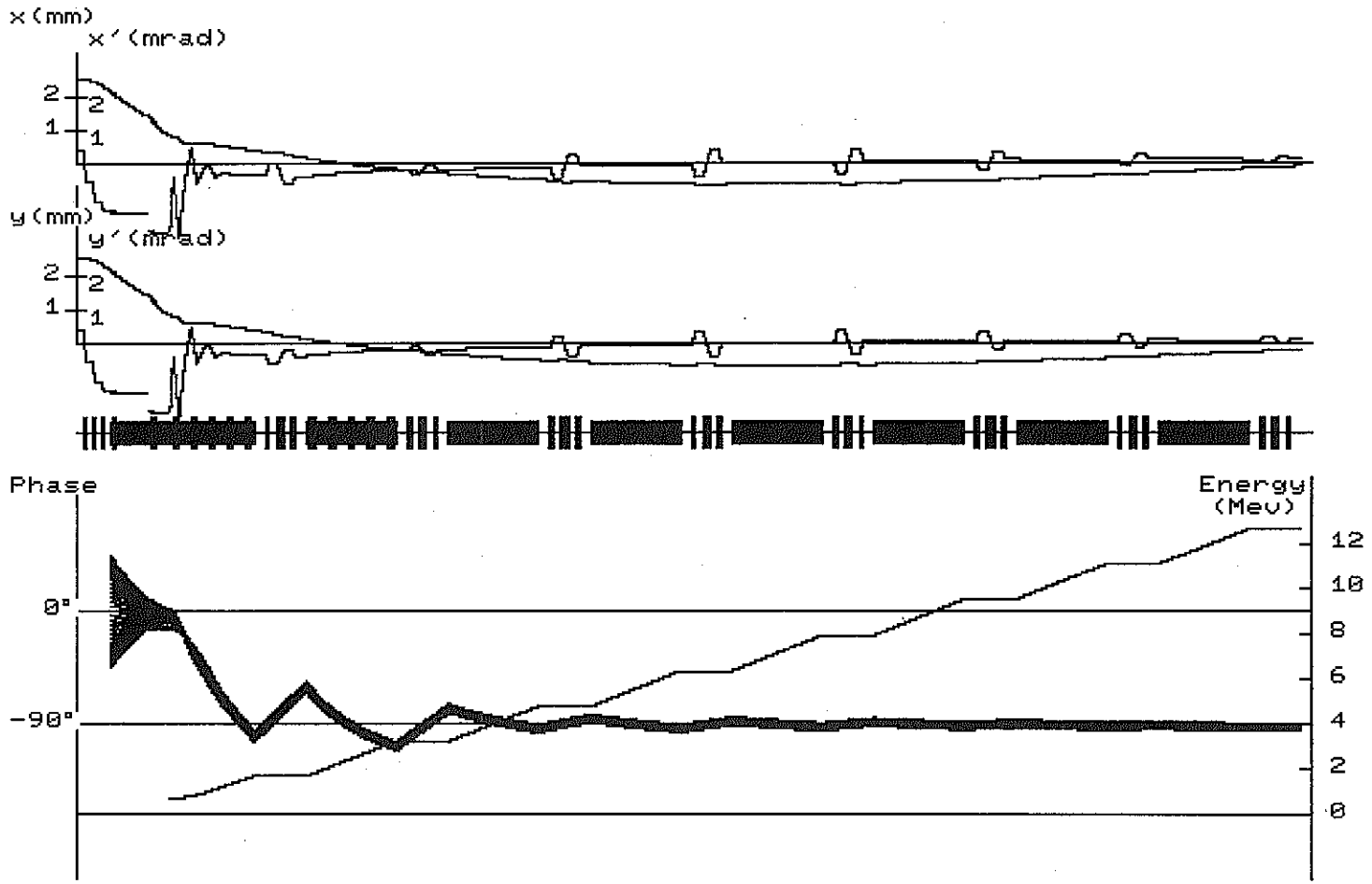

Fig. 17. The longitudinal dynamics and transverse motions of electrons by calculation

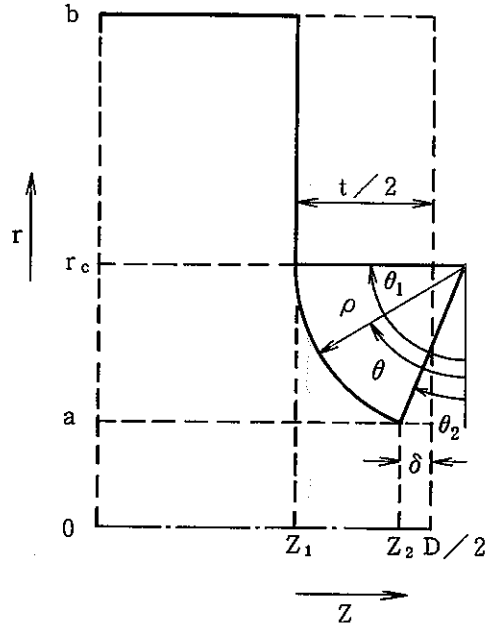

2 δ =flat land in disk hole
ρ =edge radius
t =disk thickness
2 a =disk-hole diameter
2 b =inside cylinder diameter
D =disk spacing
γ_c =radius of interface

Cross-section of a half cell of disk-loaded waveguide with rounding curvature center

slightly off the middle plane of the disk to allow a smooth tangent at $\gamma = \gamma_c$.

Fig. 18, The disk-loaded accelerator structure